

# Identification of Mobility-Resolved *N*-Glycan Isomers

Ahmed Ben Faleh, Stephan Warnke, Priyanka Bansal, Robert P. Pellegrinelli, Irina Dyukova, and Thomas R. Rizzo\*



Cite This: *Anal. Chem.* 2022, 94, 10101–10108



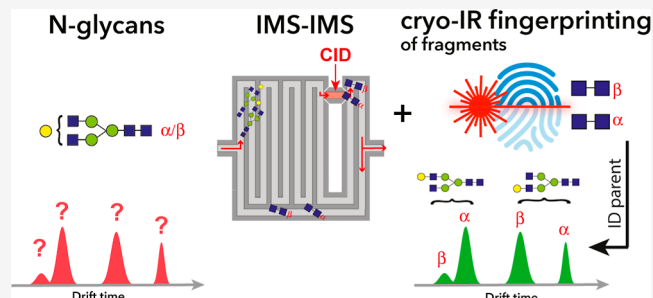
Read Online

ACCESS |

Metrics & More

Article Recommendations

**ABSTRACT:** Glycan analysis has evolved considerably during the last decade. The advent of high-resolution ion-mobility spectrometry has enabled the separation of isomers with only the slightest of structural differences. However, the ability to separate such species raises the problem of identifying all the mobility-resolved peaks that are observed, especially when analytical standards are not available. In this work, we report an approach based on the combination of IMS<sup>n</sup> with cryogenic vibrational spectroscopy to identify *N*-glycan reducing-end anomers. By identifying the reducing-end  $\alpha$  and  $\beta$  anomers of diacetyl-chitobiose, which is a disaccharide that forms part of the common core of all *N*-glycans, we are able to assign mobility peaks to reducing anomers of a selection of *N*-glycans of different sizes, starting from trisaccharides such as Man-1 up to glycans containing nine monosaccharide units, such as G2. By building an infrared fingerprint database of the identified *N*-glycans, our approach allows unambiguous identification of mobility peaks corresponding to reducing-end anomers and distinguishes them from positional isomers that might be present in a complex mixture.



## INTRODUCTION

Glycosylation is one of the most common post-translational modifications of proteins and plays a central role in their functioning. For example, the glycosylation pattern of biological drugs, such as monoclonal antibodies, directly affects their efficacy, toxicity, and shelf life and is considered a critical quality attribute by regulatory agencies.<sup>1,2</sup> Changes in the glycosylation pattern of cell-surface proteins have been used as biomarkers for breast, colon, and ovarian cancer; liver disease; and neurodegenerative diseases such as Alzheimer's and Parkinson's.<sup>3–9</sup>

Despite their biological importance, glycans represent one of the most difficult classes of molecules to analyze, arising from the isomeric complexity of their monosaccharide building blocks as well as the stereochemistry of the glycosidic linkages. While nuclear magnetic resonance (NMR) can provide information on glycan primary structure and stereochemistry, its application requires sufficient quantities of pure samples, which is often challenging to obtain.<sup>10</sup> Liquid chromatography coupled with mass spectrometry (LC-MS) has been considered the workhorse technique for the analysis of complex glycan samples owing to its high sensitivity.<sup>11,12</sup> Nevertheless, LC-MS workflows are not sufficient to separate and identify all glycan isomers unambiguously.<sup>13</sup> In addition, long LC measurement times, together with the required sample derivatization steps, limit its throughput.

High-resolution ion-mobility spectrometry (HR-IMS), on the other hand, is capable of separating glycan isomers with the

slightest structural differences on the timescale of milliseconds.<sup>14–17</sup> Combined with fragmentation techniques such as collision-induced dissociation (CID), IMS<sup>n</sup> approaches have shown great promise for glycan isomer identification.<sup>15,17–19</sup> However, the unambiguous identification of glycans based solely on the drift time or collisional cross section (CCS) remains challenging. The measured drift times depend upon the experimental conditions (pressure, temperature, voltages, etc.), which can be difficult to control with high precision, especially in the case of the highest resolution IMS techniques that use extended separation paths. The high resolving power of such techniques introduces a new caveat to data interpretation, especially when working with non-derivatized glycans because it allows the separation of not only structural isomers but also the  $\alpha$  and  $\beta$  reducing-end anomers of each isomer as well as different conformers.<sup>15–17,20</sup> In this case, a given isomer may present several peaks in its arrival-time distribution (ATD). The situation becomes even more problematic when analyzing unknown samples, where the presence of several isomeric species is possible, and the corresponding analytical standards are not necessarily available.

Received: March 16, 2022

Accepted: June 24, 2022

Published: July 7, 2022



Although an experimentally determined CCS value can indicate the presence of a given isomer, there is no guarantee that this value is unique. A CCS-based identification scheme for either parent glycans or their fragments would thus require a database including standards of all possible isomeric configurations of the molecule in question, which is clearly not practical.

Over the last few years, several groups have reported the use of infrared (IR) spectroscopy, either at room temperature<sup>21–23</sup> or at cryogenic temperatures,<sup>16,18–20,24–29</sup> for the analysis of glycan isomers. In contrast to identification based on drift times or CCS values, an IR spectrum is an inherent property of the analyte molecule, resulting in a vibrational fingerprint unique to a given isomer. If the IR fingerprint of a compound has been previously recorded and added to a database, this species can be identified without the need for spectra of all possible isomeric structures to exclude their presence. However, while an IR fingerprinting approach requires isomerically pure analytical standards only once, this still presents a problem because they are often expensive or simply not available. Without a prior isomer separation step or an isomer-specific detection scheme, in many cases it may be impossible to measure isomerically pure IR fingerprint spectra.

We have recently combined cryogenic messenger-tagging IR spectroscopy with HR-IMS isomer separation to produce highly resolved IR fingerprints of isomeric glycan structures<sup>16,24,25,27,30</sup> and in some cases, we can acquire them in as little as 10 s. While one can use this approach to identify glycans for which IR fingerprints have been previously recorded, it cannot identify molecules for which database entries do not exist. To address this issue, we have developed a workflow that combines (IMS)<sup>n</sup> with cryogenic IR fingerprinting and allows us to reconstruct the structure of unknown *N*-glycan positional isomers based on the mobility and IR fingerprints of their CID fragments.<sup>31</sup> In addition to providing a means to identify unknown glycan structures, it allows us to extend our glycan IR fingerprint database with a minimal need for analytical standards.

In the present report, we build on this work and present a procedure for assigning all major drift peaks in the ATD of a selection of *N*-glycans obtained by ultrahigh-resolution IMS. Our method is based on the identification of diagnostic fragments that allows one to determine the precise isomeric form of the precursor molecule. One molecule that is central to this approach is the disaccharide GlcNAc- $\beta$ (1–4)-GlcNAc, also called diacetyl-chitobiose, which is present at the reducing end of all *N*-linked glycans. Identification of the  $\alpha$  and  $\beta$  anomers of diacetyl-chitobiose allows us to assign certain peaks in the ATD of virtually all *N*-glycans to their respective reducing-end anomers. This, in turn, allows us to distinguish anomers of a certain isomer from other isomeric forms.

## EXPERIMENTAL SECTION

### Ion-Mobility-Selective Cryogenic IR Spectroscopy.

The experiments described in this work were performed using a home-built instrument described in detail elsewhere.<sup>20</sup> It combines high-resolution cyclic travelling-wave (TW) IMS using structures for lossless ion manipulations (SLIM)<sup>32–37</sup> with cryogenic messenger-tagging IR spectroscopy. We have incorporated a CID section within the IMS module to allow “on-board” (IMS)<sup>n</sup> experiments.<sup>18</sup> Ions are produced by a nano-electrospray source, transferred into vacuum via a stainless-steel capillary, and guided toward the IMS module

by a dual funnel assembly (MassTech). Ions are collected in a 2 m accumulation section of the SLIM IMS device prior to being introduced as packets (i.e., pulses  $\sim 100 \mu\text{s}$ –2 ms) into a 10 m serpentine separation path. The TW potentials applied to the SLIM device propel the ions through 2.2 mbar of  $\text{N}_2$  drift gas. We determine the resolving power ( $R$ ) as a function of the drift length using the reverse-sequence peptides GRGDS and SDGRG (Figure 1b).<sup>20</sup> A single-cycle separation path (10 m)

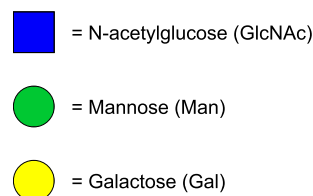


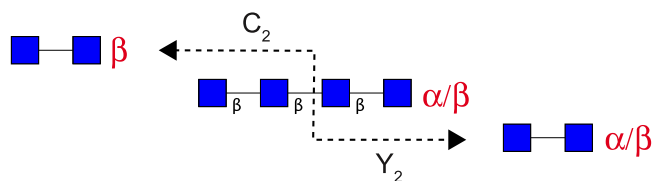
**Figure 1.** Symbols for the monosaccharides comprising the glycans discussed in this work.

provides a resolution of  $R \sim 200$ , and this increases to  $\sim 1000$  after 20 cycles.<sup>20</sup> After separation, the ions are guided through several differential pumping stages toward a cryogenic ion trap maintained at a temperature of 45 K. A few milliseconds prior to the arrival of an ion packet, a gas pulse (80:20 He/ $\text{N}_2$ ) is introduced into the trap to help confine and cool the ions. During this process, weakly bound clusters are formed between the analyte ions and  $\text{N}_2$ , with the latter serving as a messenger tag for spectroscopic interrogation.<sup>38,39</sup> A continuous, mid-IR, fiber-pumped laser (CLT series, IPG, USA) operated at 1 W power is used to irradiate the  $\text{N}_2$ -tagged analyte ions for the entirety of their trapping time (50 ms). At the end of each cycle, trapped ions are released and transferred into a TOF mass spectrometer (ToFWerk). The absorption of a resonant photon by the weakly bound clusters leads to the loss of the  $\text{N}_2$  tag, resulting in a decrease in the tagged-ion signal and an increase in that of the untagged ions. The IR spectrum of the analyte molecule is measured by monitoring the tagging yield as a function of the laser wavenumber.

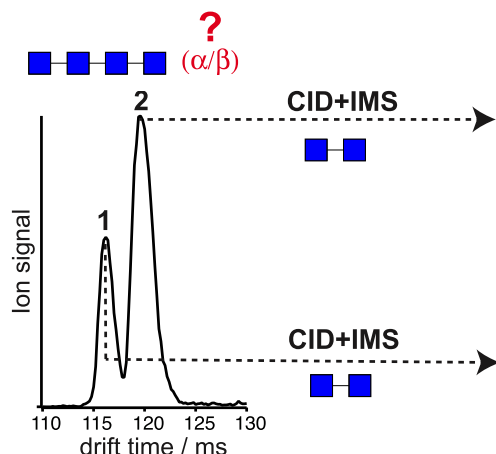
**(IMS)<sup>n</sup> Experiments.** Our SLIM IMS module includes a trapping/CID section, which allows (IMS)<sup>n</sup>-type experiments.<sup>18</sup> Compared to our first design,<sup>18</sup> we have added a dual wire-grid assembly at the entrance of the SLIM trap, increasing the fragmentation efficiency. After being separated by their mobility along the 10 m serpentine path, parent ions are introduced into the trapping region, which is held at a bias voltage lower than that of the rest of the IMS device. As these ions pass through the grid system at the trap entrance, they experience a homogenous electric field of up to 3300 V/cm, which induces them to undergo energetic collisions with  $\text{N}_2$ , causing them to dissociate. The resulting fragments are then released from the trap and sent for additional separation cycles on the IMS device before being directed to the cryogenic ion trap, hence allowing for the acquisition of IR spectra of mobility separated fragments. We recently demonstrated the use of this method to identify *N*-glycan positional isomers.<sup>31</sup>

**Identification of Drift Peaks Corresponding to *N*-Glycan Isomers.** Our approach for isomer identification and database construction has been described in detail recently.<sup>31</sup> In brief, different glycan isomers are initially separated according to their respective mobilities. Each separated isomer is then subjected to CID, producing a range of fragments. Those that are diagnostic for the structure of their precursor molecules are subsequently mobility-separated and their IR

## a) CID fragmentation scheme



## b) ATD of tetraacetyl-chitotetraose



## c) ATDs of chitobiose CID fragments

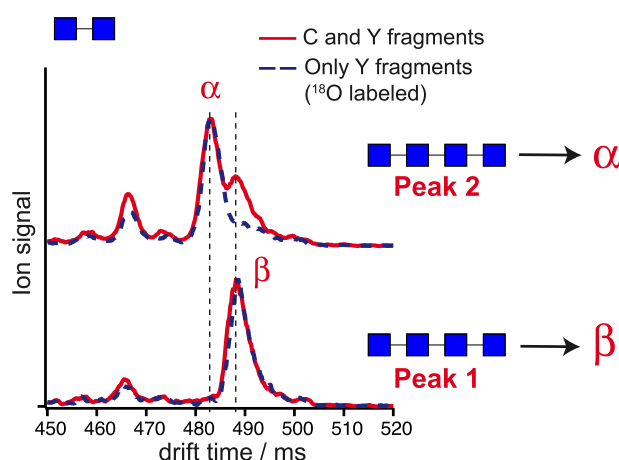


**Figure 2.** (a) Fragmentation scheme for identifying diacetyl-chitobiose anomers. (b) ATD of tetraacetyl-chitotetraose after one separation cycle in the IMS device. (c) ATDs of the 447  $m/z$  fragments (red traces) and the 449  $m/z$   $^{18}\text{O}$  substituted fragments (dashed blue traces) after four separation cycles obtained from peak one (bottom panel) and peak two (top panel) of the tetrasaccharide.

fingerprints recorded. Once the isomeric fragments are identified either by their relative drift-peak position or by comparison to an IR fingerprint database, it is possible to assign the structure of the parent molecules. Using an initial database including IR fingerprints of diacetyl-chitobiose isomers, we demonstrate the ability to distinguish drift peaks corresponding to  $N$ -glycan  $\alpha$  and  $\beta$  reducing-end anomers from those of positional isomers or different gas-phase conformers. Once the reducing-end anomers of a given  $N$ -glycan are identified, their drift times and IR fingerprint spectra can in turn be used to identify larger structures. Starting from a disaccharide, we demonstrate how we can identify the reducing-end anomers of the  $N$ -glycan G2. Following this approach, we also show that once the reducing-end anomers of a structure are identified, we can determine the anomericity of all its Y fragments.

**Materials.** Man1, Man2, Man3, and Man5 glycans were purchased from Dextra. G0-N, G0, G1, and G2 glycans were purchased from TheraProtein. The diacetyl-chitobiose and tetraacetyl-chitotetraose samples were purchased from Carbo-synth. For nano-electrospray ionization (nESI), 5–20  $\mu\text{M}$  solutions of the analytes were prepared in 50/50 MeOH/ $\text{H}_2\text{O}$ . In-house prepared borosilicate glass nanospray emitters were used to inject samples into the instrument. All molecules were analyzed in their singly sodiated form. All gases were of 99.9999% purity. Symbols for the monosaccharide components comprising these glycans are given in Figure 1.

## RESULTS AND DISCUSSION

**Identification of the  $\alpha$  and  $\beta$  Reducing-End Anomers of Diacetyl-Chitobiose.** Because the disaccharide diacetyl-

chitobiose is part of the common core found at the reducing end of all  $N$ -linked glycans, we use it as the starting point for the identification of  $\alpha$  and  $\beta$  anomers. To identify the reducing-end anomers of this disaccharide, we used tetraacetyl-chitotetraose, a tetrasaccharide composed of four  $\beta(1-4)$  linked GlcNAc building blocks. A particularity of this molecule is that because all monosaccharides composing it are  $\beta$ -linked, both  $Y_2$  and  $C_2$  fragments<sup>40</sup> can provide information about the reducing-end configuration of the disaccharide diacetyl-chitobiose. As shown schematically in Figure 2a, after mobility separation of the  $\alpha$  and  $\beta$  anomers of the parent tetrasaccharide, the  $Y_2$  and  $C_2$  fragments generated from the  $\beta$  anomer should correspond to pure  $\beta$ -diacetyl-chitobiose, while the same fragments of the  $\alpha$  anomer will represent a mixture of both reducing-end anomers of the disaccharide. This hypothesis is based on the previously demonstrated anomeric retention of the glycosidic bond upon CID fragmentation.<sup>19,23</sup> An ATD of the precursor molecule tetraacetyl-chitotetraose is displayed in Figure 2b and shows two distinct mobility peaks, suggesting the presence of two reducing-end anomers. Figure 2c shows the ATDs (in red) of a mixture of  $Y_2$  and  $C_2$  fragments corresponding to diacetyl-chitobiose ( $m/z$  447) produced upon CID of the first (bottom panel) and second (top panel) drift peaks of the tetrasaccharide.

We clearly observe an additional mobility peak at 482 ms in the ATD of the fragments generated from the second mobility peak of the tetrasaccharide that is not present in the ATD of the fragments generated from the first parent mobility peak, where the main mobility feature is centered around 488 ms. As described above,  $C_2$  and  $Y_2$  fragments should be equivalent in

structure and hence yield a single mobility feature if only the  $\beta$  anomer of the parent tetrasaccharide was initially selected, while the  $C_2$  and  $Y_2$  fragments will be of the opposite anomericity and may result in two drift peaks when generated from the  $\alpha$  anomer of the parent. The mobility feature at 488 ms in Figure 2c can therefore be attributed to fragments corresponding to diacetyl-chitobiose in the  $\beta$  configuration and the feature at 482 ms to the  $\alpha$  anomeric configuration. The feature at 465 ms present in the fragment ATDs from both tetrasaccharide species possibly corresponds to open-ring structures at the reducing end, as proposed previously.<sup>14</sup>

To differentiate between the  $C_2$  and  $Y_2$  fragments, we use <sup>18</sup>O isotopically labeled tetrasaccharide. Because the substitution exclusively occurs at the reducing end, it will appear only in the Y fragments. The ATDs of isolated Y fragments should therefore represent the arrival times of pure  $\alpha$  or  $\beta$  reducing-end anomers, depending on which anomer was selected for CID. These ATDs are shown as blue dotted lines in Figure 2c, and indeed each displays a single peak in the region of 480 to 500 ms, supporting our assignment of the two drift peaks to the two reducing-end anomers of fragments corresponding to diacetyl-chitobiose, with the  $\alpha$  anomer being slightly more mobile than the  $\beta$  anomer. This distinction in mobility will later be used to assign anomers of larger species.

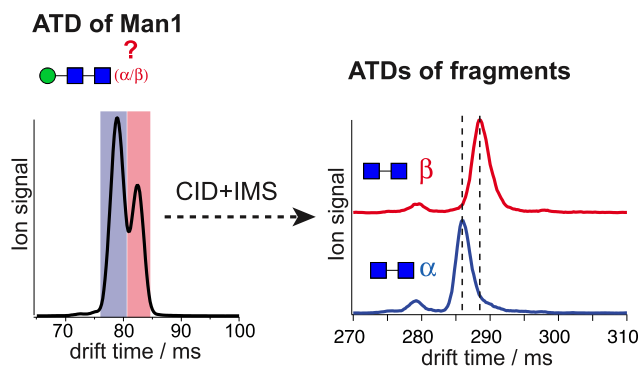
Once identified, the IR fingerprints of the  $\alpha$  and  $\beta$  anomers of diacetyl-chitobiose were recorded and stored in our database (gray spectra in Figure 4b).

**Identification of High-Mannose Glycan Drift Peaks Based on Fragment Mobilities.** We can use the information obtained on diacetyl-chitobiose anomers to identify the drift peaks corresponding to the  $\alpha$  and  $\beta$  reducing-end anomers of high-mannose glycans. To do so, we follow the same protocol as described earlier: we separate the molecules of interest according to their mobility using IMS and then fragment the separated isomers into diacetyl-chitobiose, for which the mobility of the reducing-end anomers has been previously determined.

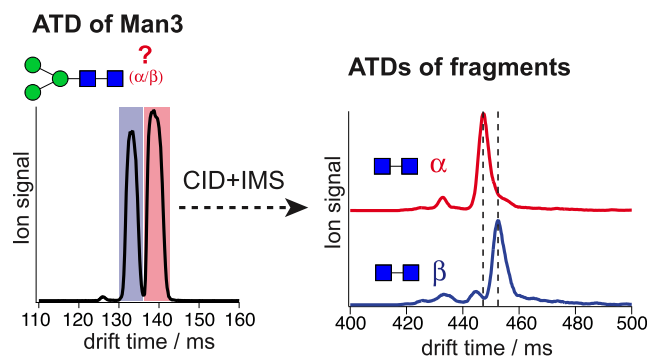
Figure 3 shows the results obtained for different high-mannose *N*-glycans. In each case, the left panels depict the ATDs of the parent molecules after one IMS separation cycle, while the right panels show the ATDs of the 447 *m/z* fragments generated from the first (blue) and second (red) parent mobility feature after three additional IMS separation cycles. In the present case, it is possible to unambiguously assign  $\alpha$  and  $\beta$  reducing-end anomers based on the relative position of the fragment drift peaks because diacetyl-chitobiose is the only one with *m/z* 447. The ATDs of the *m/z* 447 fragments shown in Figure 3 resemble those of the diacetyl-chitobiose species in Figure 2, where we assigned the earlier drift feature to the  $\alpha$  anomer and the later peak to the  $\beta$  anomer. We can thus assign the first peak in the ATD of Man1 to the  $\alpha$  reducing-end anomer and the second peak to the  $\beta$  anomer. The reverse order was found for both Man3 and Man5 where the first and second drift peaks correspond to the  $\beta$  and  $\alpha$  anomers, respectively.

**Identification of G0-N(3) Drift Peaks Based on Fragment IR Fingerprinting.** In addition to using ATDs of CID fragments to identify peaks in the ATD of parent glycans, we can also use fragment IR fingerprints. Using G0-N(3) (which has the non-reducing GlcNAc on the  $\alpha$ -3 branch as in Figure 4a) as an example, we first separate isomers of the parent molecules by their mobility.

### a) Assignment of Man1 reducing-end anomers



### b) Assignment of Man3 reducing-end anomers



### c) Assignment of Man5 reducing-end anomers

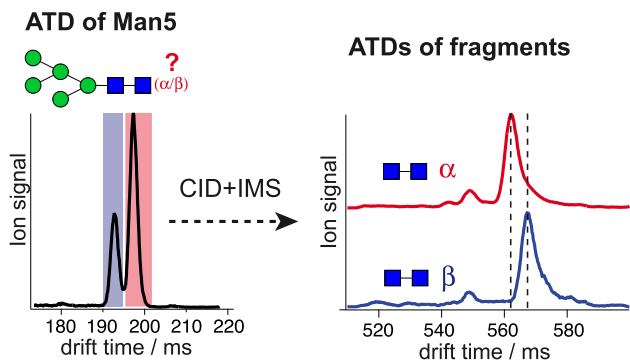


**Figure 3.** (a) (left panel) ATD of Man1 after one IMS separation cycle; (right panel) ATDs of the diacetyl-chitobiose fragments produced by CID from peak 1 (blue) and peak 2 (red) of Man1, after three IMS separation cycles. (b) (left panel) ATD of Man3 after one IMS separation cycle and (right panel) ATDs of the diacetyl-chitobiose fragments produced from peak 1 (blue) and peak 2 (red) of Man3, after three IMS separation cycles. (c) (left panel) ATD of Man5 after one IMS separation cycle and (right panel) ATDs of the diacetyl-chitobiose fragments produced from peak 1 (blue) and peak 2 (red) of Man5, after three IMS separation cycles. The differences in the absolute drift time of diacetyl-chitobiose obtained when fragmenting different molecules is due to different conditions needed for the optimal separation of the parent ions.

The ATD of G0-N(3) after one separation cycle is displayed in Figure 4a and exhibits two drift peaks. Using CID, we produced *m/z* 447 fragments (corresponding to diacetyl-chitobiose) separately for each mobility peak of G0-N(3) and recorded their corresponding IR spectra. Figure 4b shows the

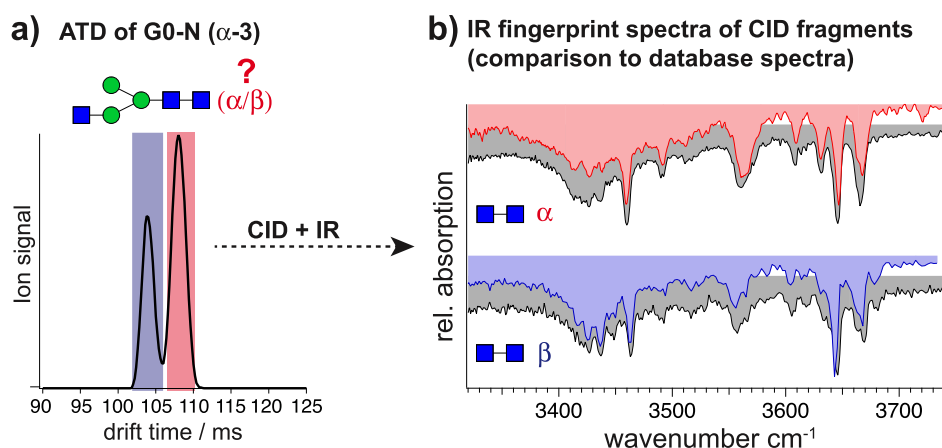


**Figure 4.** (a) ATD of G0-N(3) after one IMS separation cycle. (b) IR spectral comparison of CID fragments corresponding to diacetyl-chitobiose produced from peak one (blue) and peak two (red) of G0-N(3), to previously recorded database IR spectra of  $\alpha$  (top panel, gray) and  $\beta$  (bottom panel, gray) reducing-end anomers of diacetyl-chitobiose.

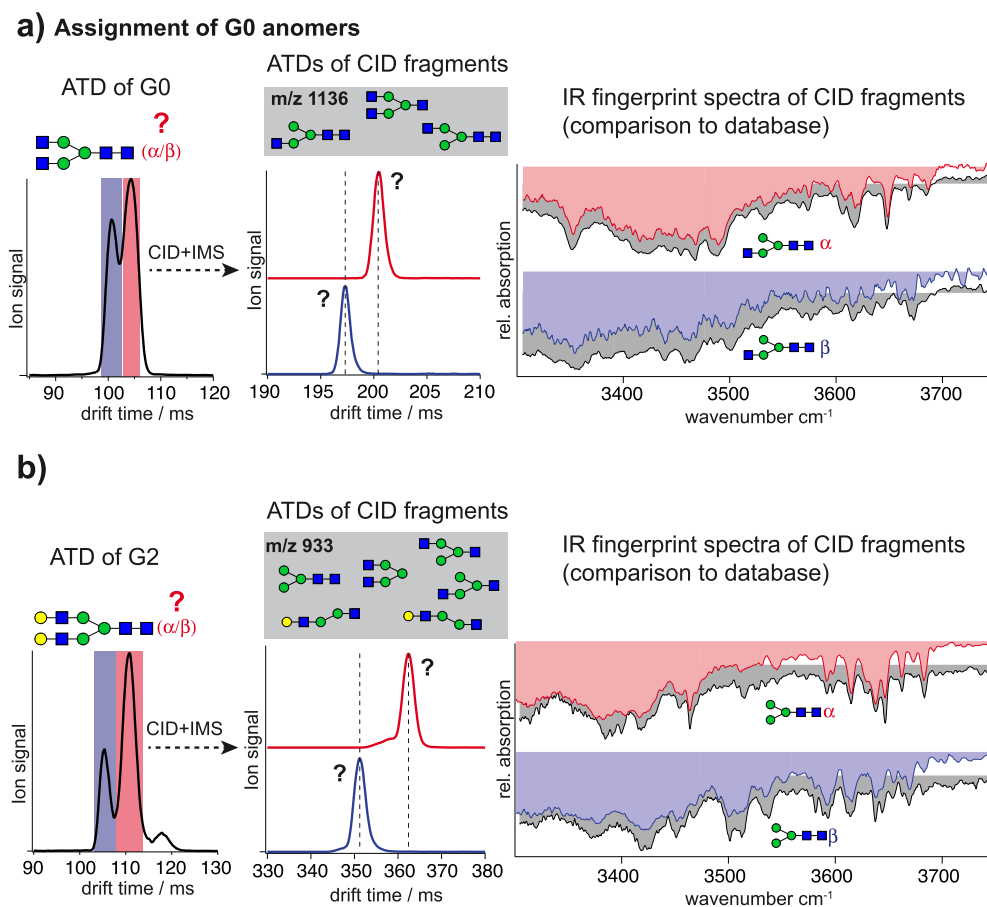


**Figure 5.** (a) (left panel) ATD of G0 after one IMS separation cycle; (middle panel) ATDs of G0-N(3) fragments produced from peak 1 (blue) and peak 2 (red) of G0 after one IMS separation cycle; and (right panel) IR spectral comparison of G0-N(3) fragments produced from peak 1 (blue) and peak 2 (red) of G0 to previously recorded database IR spectra of  $\alpha$  (gray, top) and  $\beta$  (gray, bottom) reducing-end anomers of G0-N(3) and (b) (left panel) ATD of G2 after one IMS separation cycle; (middle panel) ATDs of Man3 fragments produced from peak 1 (blue) and peak 2 (red) of G2 after 2 IMS separation cycles; (right panel) IR spectral comparison of Man3 fragments produced from peak 1 (blue) and peak 2 (red) of G2, to previously recorded database IR spectra of  $\alpha$  (gray, top) and  $\beta$  (gray, bottom) reducing-end anomers of Man3.

comparison of these spectra with the previously recorded IR fingerprints for the  $\alpha$  and  $\beta$  diacetyl-chitobiose reducing-end anomers (displayed in gray), which confirms that the fragments produced from peak 1 of G0-N(3) correspond to  $\beta$  diacetyl-chitobiose, while the one produced from peak 2 corresponds to  $\alpha$  diacetyl-chitobiose. It is worth noting that the

main differences between the IR fingerprints of the  $\alpha$  and  $\beta$  diacetyl-chitobiose reducing-end isomers lie within the structure of the absorptions at  $3646\text{ cm}^{-1}$ , as well as in the intensity of the absorption at  $3463\text{ cm}^{-1}$ . We can thus assign the first and second drift peaks of G0-N(3) to its  $\beta$  and  $\alpha$  reducing-end anomers, respectively.

**Identification of Hybrid *N*-Glycan Drift Peaks by Fragment IR Fingerprinting.** Using the information obtained in the experiments described above, we can assign the drift peaks of larger hybrid *N*-glycans. Here, we use glycan fragments corresponding to G0-N(3) and Man3 to assign the drift peaks of the *N*-glycans G0 and G2, respectively. The ATD displayed in Figure 5a (left) shows two major drift peaks after a single-cycle IMS separation, corresponding to two isomers of G0. One of the main fragments observed for these ions has an  $m/z$  of 1136. As displayed in the middle panel of Figure 5a, several structures can give rise to this particular  $m/z$ , including G0-N(3), G0-N(6), and G0-core N resulting from the loss of one GlcNAc at the reducing end. In this case, we use IR spectroscopy to identify, which of these fragments are produced. The spectra are shown in the right-hand panel of Figure 5a for fragments generated from the first drift peak of G0 (blue) and for the second drift peak (red). A comparison to previously recorded database IR fingerprints of G0-N(3) reducing-end anomers (shown in gray) identifies fragments from the first drift peak of G0 as the  $\beta$  anomer of G0-N(3) and fragments from the second drift peak as the  $\alpha$  anomer of the same molecule. Because the reducing-end anomericity does not change upon CID, we can thus assign the first drift peak of G0 to  $\beta$  anomers and the second drift peak to its  $\alpha$  anomer.

Following the same protocol and looking at Man3 fragments, we can assign the first and second peaks of G2 to its  $\beta$  and  $\alpha$  reducing-end anomers, respectively. This example illustrates the utility of IR fingerprinting, because to identify the fragments exclusively on the basis of their drift times would require a database with ion-mobility entries for all six possible fragments corresponding to  $m/z$  933. In contrast, as shown in the right-hand panel of Figure 5b, the IR fingerprints of these fragments provide a positive match for the Man3 reducing-end anomers, which allows the assignment of the observed fragments to their corresponding structures without the need for reference IR fingerprints of all possible alternatives.

**Identification of *N*-Glycan Fragment Isomers.** The *N*-glycan drift peak identification method presented above has been based on the assignment of drift peaks to isomers of structurally diagnostic fragments. In a reverse application of the presented workflow, it is also possible to obtain information about the isomeric nature of other fragments once the drift peaks observed for a given precursor molecule have been assigned to specific isomers. To illustrate this approach, we chose the *N*-glycan G2 for which we have identified the reducing-end anomeric configuration of the main drift peaks in the ATD of Figure 5b using Man3 as structurally diagnostic fragments.

Starting from the same ATD of G2, we can generate fragments of  $m/z$  1501 (corresponding to the glycan G1) from each of the two identified drift peaks and subject them to two additional separation cycles. The result, which is displayed in Figure 6a, shows two distinct drift peaks for fragments corresponding to G1 generated from either  $\alpha$  (top panel) or  $\beta$  (bottom panel) anomeric precursor ions. Following a similar fragment-based identification protocol, we have recently demonstrated that the first two drift peaks in the ATD of G1 (i.e., in the region of 375–390 ms) correspond to the G1(6) positional isomer, in which the terminal galactose is located on the upper branch, while the last two drift peaks (410–425 ms) correspond to the G1(3) positional isomers with the terminal galactose on the lower branch.<sup>31</sup> Using this information, we can assign every major drift peak in the ATD

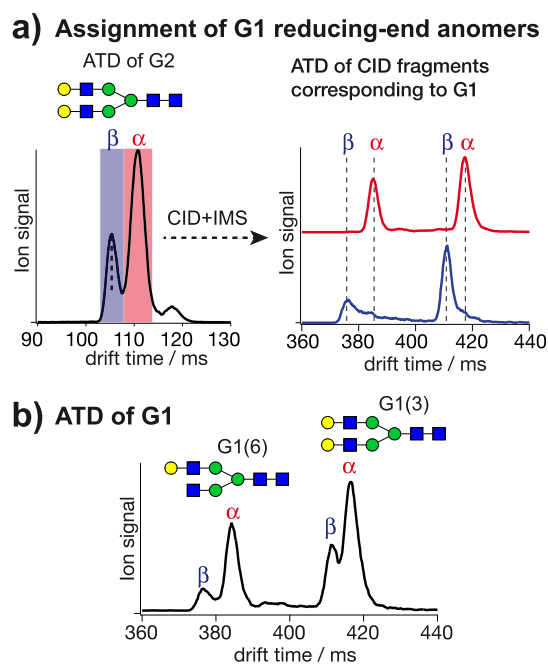


**Figure 6.** (a) (left panel) ATD of G2 after one IMS separation cycle and (right panel) ATDs of the G1 fragments produced from peak 1 (blue) and peak 2 (red) of G2 after two IMS separation cycles. (b) ATD of G1 after two separation cycles with the assignment of  $\alpha$ -3 and  $\alpha$ -6 positional isomers and their respective reducing-end anomers.

of G1 to the corresponding isomer as well as their reducing-end anomeric configuration, as shown in Figure 6b.

If we go one step further and add IR fingerprint spectroscopy to the (IMS)<sup>n</sup> schemes described above, we can access and identify isomers of fragments that are challenging to separate by their mobility. To illustrate this, we used Man2(6) as an example. After up to 10 separation cycles in our IMS device (~100 m drift path), it was not possible to separate the Man2(6) reducing-end anomers. However, using G0-N(3) as precursor ions for which reducing-end anomers can be separated and identified, it is possible to obtain the  $\alpha$  and  $\beta$  reducing-end anomers of Man2(6) as fragments.

After mobility separation of G0-N(3) and identification of its reducing-end anomers, as shown in Figure 4a, we selectively perform CID on the separated drift peaks to obtain fragments corresponding to Man2(6) ( $m/z$  771). These Man2(6) ions now have a defined reducing-end anomericity, and we can obtain an IR fingerprint for the  $\alpha$  and  $\beta$  reducing end-anomers (Figure 7b). These, in turn, can serve as structurally diagnostic fragments to identify positional isomers and anomers of larger unknown structures. It is interesting to note the similarity of the IR spectra of the  $\alpha$  and  $\beta$  anomers of Man2(6), with only slight differences occurring in the region 3630–3660  $\text{cm}^{-1}$ . This is consistent with the fact that these anomers are difficult to separate by ion mobility.

## CONCLUSIONS

The glycan sequencing approach presented in this work highlights the complementarity between HR-IMS and cryogenic IR spectroscopy. Notably, IMS<sup>n</sup> offers richer information about the isomeric nature of glycans and their fragments compared to MS<sup>n</sup> alone and can be sufficient for identifying glycan structures in the cases where the number of

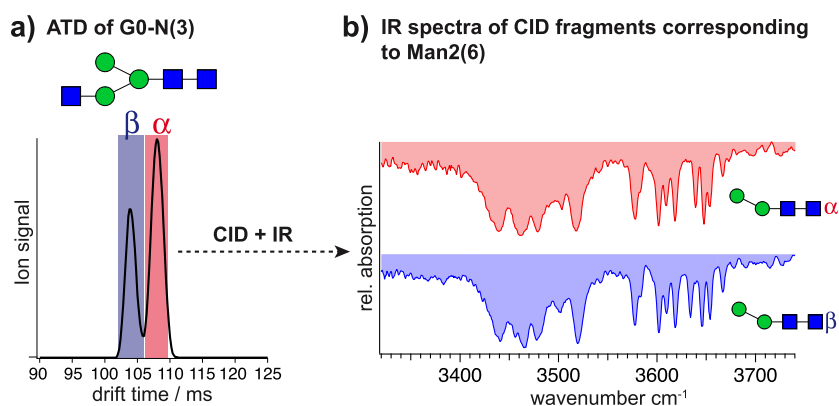


**Figure 7.** (a) ATD of G0-N(3) after one IMS separation cycle. (b) IR fingerprints of Man2 fragments from G0-N(3)  $\alpha$  reducing-end anomer (top spectrum, red) and G0-N(3)  $\beta$  reducing-end anomer (bottom spectrum, blue).

possible fragment isomers is limited, the IMS resolving power is high enough to separate isomers, and a drift-time calibration is accurate enough to discern a specific species. Nevertheless, when working with complex structures, it is often the case that a fragment mass-to-charge ratio corresponds to more than one isomer, as shown in the examples in Figure 5. In this case, IMS<sup>n</sup> alone fails to provide an unambiguous assignment of the glycan structure without: (a) a database containing mobility information about all possible isomers of the observed fragment; (b) the ability to separate them by mobility; and (c) an accurate and reproducible determination of CCS values. The latter is extremely challenging to obtain under ultrahigh-resolution IMS conditions<sup>41,42</sup> and obtaining the required pure analytical standards for all possible fragment isomers in question is impractical. In contrast, using cryogenic IR spectroscopy, it is possible to unambiguously assign a structure based on its unique IR fingerprint alone without the need for drift-time calibration.

The combination of IMS<sup>n</sup> with cryogenic IR spectroscopy can thus be used to determine the identity of drift peaks separated using HR-IMS, as well as to produce isomerically pure IR fingerprints of glycans for which pure analytical standards are not available. This approach, demonstrated here on N-glycans, can be generalized to other classes of glycans that have common-core structures, such as complex human milk oligosaccharides or O-linked glycans, as well as other classes of biomolecules such as metabolites and lipids. The work performed here suggests that the combination of IMS<sup>n</sup> with IR fingerprinting has the potential to have a major impact in fields where the identification of the slightest structural differences is crucial, such as drug development, disease biomarker research, or forensics.

## AUTHOR INFORMATION

### Corresponding Author

**Thomas R. Rizzo** – Laboratoire de Chimie Physique Moléculaire, EPFL SB ISIC LCPM, École Polytechnique Fédérale de Lausanne, Lausanne CH-1015, Switzerland; [orcid.org/0000-0003-2796-905X](https://orcid.org/0000-0003-2796-905X); Email: [thomas.rizzo@epfl.ch](mailto:thomas.rizzo@epfl.ch)

### Authors

**Ahmed Ben Faleh** – Laboratoire de Chimie Physique Moléculaire, EPFL SB ISIC LCPM, École Polytechnique Fédérale de Lausanne, Lausanne CH-1015, Switzerland; [orcid.org/0000-0002-9144-2052](https://orcid.org/0000-0002-9144-2052)

**Stephan Warnke** – Laboratoire de Chimie Physique Moléculaire, EPFL SB ISIC LCPM, École Polytechnique Fédérale de Lausanne, Lausanne CH-1015, Switzerland; [orcid.org/0000-0001-7481-286X](https://orcid.org/0000-0001-7481-286X)

**Priyanka Bansal** – Laboratoire de Chimie Physique Moléculaire, EPFL SB ISIC LCPM, École Polytechnique Fédérale de Lausanne, Lausanne CH-1015, Switzerland

**Robert P. Pellegrinelli** – Laboratoire de Chimie Physique Moléculaire, EPFL SB ISIC LCPM, École Polytechnique Fédérale de Lausanne, Lausanne CH-1015, Switzerland

**Irina Dyukova** – Laboratoire de Chimie Physique Moléculaire, EPFL SB ISIC LCPM, École Polytechnique Fédérale de Lausanne, Lausanne CH-1015, Switzerland

Complete contact information is available at: <https://pubs.acs.org/10.1021/acs.analchem.2c01181>

## Notes

The authors declare no competing financial interest.

## ACKNOWLEDGMENTS

The authors thank the European Research Council (grant 788697-GLYCANAL) and the Swiss National Science Foundation (grants 200020\_184838 and 206021\_177004) for their support of this work.

## REFERENCES

- (1) Valverde, P.; Ardá, A.; Reichardt, N.-C.; Jiménez-Barbero, J.; Gimeno, A. *Medchemcomm* **2019**, *10*, 1678–1691.
- (2) Lemery, S. J.; Ricci, M. S.; Keegan, P.; McKee, A. E.; Pazdur, R. *Clin. Cancer Res.* **2017**, *23*, 1882–1885.
- (3) Adamczyk, B.; Tharmalingam, T.; Rudd, P. M. *Biochim. Biophys. Acta* **2012**, *1820*, 1347–1353.
- (4) Leiserowitz, G. S.; Lebrilla, C.; Miyamoto, S.; An, H. J.; Duong, H.; Kirmiz, C.; Li, B.; Liu, H.; Lam, K. S. *Int. J. Gynecol. Cancer* **2008**, *18*, 470–475.
- (5) Mayeux, R. *Neurotherapeutics* **2004**, *1*, 182–188.
- (6) Palmigiano, A.; Barone, R.; Sturiale, L.; Sanfilippo, C.; Bua, R. O.; Romeo, D. A.; Messina, A.; Capuana, M. L.; Maci, T.; Le Pira, F.; Zappia, M.; Garozzo, D. *J. Proteomics* **2016**, *131*, 29–37.
- (7) Russell, A. C.; Šimurina, M.; Garcia, M. T.; Novokmet, M.; Wang, Y.; Rudan, I.; Campbell, H.; Lauc, G.; Thomas, M. G.; Wang, W. *Glycobiology* **2017**, *27*, 501–510.
- (8) Wong, C.-H.; Taniguchi, N. Current Status and New Challenges in Glycoscience: Overview. In *Glycoscience: Biology and Medicine*; Taniguchi, N., Endo, T., Hart, G. W., Seeberger, P. H., Wong, C.-H., Eds.; Springer Japan: Tokyo, 2015; pp 11–14.

- (9) Dube, D. H.; Bertozzi, C. R. *Nat. Rev. Drug Discovery* **2005**, *4*, 477–488.
- (10) Lundborg, M.; Fontana, C.; Widmalm, G. *Biomacromolecules* **2011**, *12*, 3851–3855.
- (11) Nagy, G.; Peng, T.; Pohl, N. L. B. *Anal. Methods* **2017**, *9*, 3579–3593.
- (12) Mariño, K.; Bones, J.; Kattla, J. J.; Rudd, P. M. *Nat. Chem. Biol.* **2010**, *6*, 713–723.
- (13) Vreeker, G. C. M.; Wuhrer, M. *Anal. Bioanal. Chem.* **2017**, *409*, 359–378.
- (14) Nagy, G.; Attah, I. K.; Garimella, S. V. B.; Tang, K.; Ibrahim, Y. M.; Baker, E. S.; Smith, R. D. *Chem. Commun.* **2018**, *54*, 11701–11704.
- (15) Ujma, J.; Ropartz, D.; Giles, K.; Richardson, K.; Langridge, D.; Wildgoose, J.; Green, M.; Pringle, S. J. *Am. Soc. Mass Spectrom.* **2019**, *30*, 1028–1037.
- (16) Warnke, S.; Ben Faleh, A.; Scutelnic, V.; Rizzo, T. R. *J. Am. Soc. Mass Spectrom.* **2019**, *30*, 2204–2211.
- (17) Peterson, T. L.; Nagy, G. *Anal. Chem.* **2021**, *93*, 9397–9407.
- (18) Bansal, P.; Yatsyna, V.; AbiKhodr, A. H.; Warnke, S.; Ben Faleh, A.; Yalovenko, N.; Wysocki, V. H.; Rizzo, T. R. *Anal. Chem.* **2020**, *92*, 9079–9085.
- (19) Pellegrinelli, R. P.; Yue, L.; Carrascosa, E.; Warnke, S.; Ben Faleh, A.; Rizzo, T. R. *J. Am. Chem. Soc.* **2020**, *142*, 5948–5951.
- (20) Warnke, S.; Ben Faleh, A.; Rizzo, T. R. *ACS Meas. Sci. Au* **2021**, *1*, 157–164.
- (21) Barnes, L.; Schindler, B.; Chambert, S.; Allouche, A.-R.; Compagnon, I. *Int. J. Mass Spectrom.* **2017**, *421*, 116–123.
- (22) Schindler, B.; Barnes, L.; Gray, C. J.; Chambert, S.; Flitsch, S. L.; Oomens, J.; Daniel, R.; Allouche, A. R.; Compagnon, I. *J. Phys. Chem. A* **2017**, *121*, 2114–2120.
- (23) Schindler, B.; Barnes, L.; Renois, G.; Gray, C.; Chambert, S.; Fort, S.; Flitsch, S.; Loison, C.; Allouche, A.-R.; Compagnon, I. *Nat. Commun.* **2017**, *8*, 1–7.
- (24) Abikhodr, A. H.; Yatsyna, V.; Ben Faleh, A.; Warnke, S.; Rizzo, T. R. *Anal. Chem.* **2021**, *93*, 14730–14736.
- (25) Ben Faleh, A.; Warnke, S.; Rizzo, T. R. *Anal. Chem.* **2019**, *91*, 4876–4882.
- (26) Dyukova, I.; Ben Faleh, A.; Warnke, S.; Yalovenko, N.; Yatsyna, V.; Bansal, P.; Rizzo, T. R. *Analyst* **2021**, *146*, 4789–4795.
- (27) Warnke, S.; Ben Faleh, A.; Pellegrinelli, R. P.; Yalovenko, N.; Rizzo, T. R. *Faraday Discuss.* **2018**, *217*, 114–125.
- (28) Mucha, E.; González Flórez, A. I.; Marianski, M.; Thomas, D. A.; Hoffmann, W.; Struwe, W. B.; Hahm, H. S.; Gewinner, S.; Schöllkopf, W.; Seeberger, P. H.; von Helden, G.; Pagel, K. *Angew. Chem., Int. Ed.* **2017**, *56*, 11248–11251.
- (29) Mucha, E.; Stuckmann, A.; Marianski, M.; Struwe, W. B.; Meijer, G.; Pagel, K. *Chem. Sci.* **2019**, *10*, 1272–1284.
- (30) Masellis, C.; Khanal, N.; Kamrath, M. Z.; Clemmer, D. E.; Rizzo, T. R. *J. Am. Soc. Mass Spectrom.* **2017**, *28*, 2217–2222.
- (31) Bansal, P.; Ben Faleh, A.; Warnke, S.; Rizzo, T. R. *Analyst* **2022**, *147*, 704–711.
- (32) Deng, L.; Ibrahim, Y. M.; Hamid, A. M.; Garimella, S. V. B.; Webb, I. K.; Zheng, X.; Prost, S. A.; Sandoval, J. A.; Norheim, R. V.; Anderson, G. A.; Tolmachev, A. V.; Baker, E. S.; Smith, R. D. *Anal. Chem.* **2016**, *88*, 8957–8964.
- (33) Hamid, A. M.; Garimella, S. V. B.; Ibrahim, Y. M.; Deng, L.; Zheng, X.; Webb, I. K.; Anderson, G. A.; Prost, S. A.; Norheim, R. V.; Tolmachev, A. V.; Baker, E. S.; Smith, R. D. *Anal. Chem.* **2016**, *88*, 8949–8956.
- (34) Hamid, A. M.; Ibrahim, Y. M.; Garimella, S. V. B.; Webb, I. K.; Deng, L.; Chen, T.-C.; Anderson, G. A.; Prost, S. A.; Norheim, R. V.; Tolmachev, A. V.; Smith, R. D. *Anal. Chem.* **2015**, *87*, 11301–11308.
- (35) Ibrahim, Y. M.; Hamid, A. M.; Deng, L.; Garimella, S. V. B.; Webb, I. K.; Baker, E. S.; Smith, R. D. *Analyst* **2017**, *142*, 1010–1021.
- (36) Ibrahim, Y. M.; Shvartsburg, A. A.; Smith, R. D.; Belov, M. E. *Anal. Chem.* **2011**, *83*, 5617–5623.
- (37) Webb, I. K.; Garimella, S. V. B.; Norheim, R. V.; Baker, E. S.; Ibrahim, Y. M.; Smith, R. D. *J. Am. Soc. Mass Spectrom.* **2016**, *27*, 1285–1288.
- (38) Kamrath, M. Z.; Garand, E.; Jordan, P. A.; Leavitt, C. M.; Wolk, A. B.; Van Stipdonk, M. J.; Miller, S. J.; Johnson, M. A. *J. Am. Chem. Soc.* **2011**, *133*, 6440–6448.
- (39) Voss, J. M.; Kregel, S. J.; Fischer, K. C.; Garand, E. *J. Am. Soc. Mass Spectrom.* **2018**, *29*, 42–50.
- (40) Domon, B.; Costello, C. E. *Glycoconjugate J.* **1988**, *5*, 397–409.
- (41) Causon, T. J.; Hann, S. J. *Am. Soc. Mass Spectrom.* **2020**, *31*, 2102–2110.
- (42) Stow, S. M.; Causon, T. J.; Zheng, X.; Kurulugama, R. T.; Mairinger, T.; May, J. C.; Rennie, E. E.; Baker, E. S.; Smith, R. D.; McLean, J. A.; Hann, S.; Fjeldsted, J. C. *Anal. Chem.* **2017**, *89*, 9048–9055.